Hybrids of Triphenylamine-Functionalized Polyacetylenes and Multiwalled Carbon Nanotubes: High Solubility, Strong Donor−Acceptor Interaction, and Excellent Photoconductivity

Hui Zhao,[†] Wang Zhang Yuan,[†,‡] Li Tang,[†] Jing Zhi Sun,*[,†] Haipeng Xu,[†] Anjun Qin,[†,‡] Yu Mao,[†] Jia Ke Jin,[†] and Ben Zhong Tang*[,†,‡]

Department of Polymer Science and Engineering, Zhejiang University, Hangzhou 310027, China, and Department of Chemistry, The Hong Kong University of Science and Technology, Clear Water Bay, Kowloon, Hong Kong, China

Received June 26, 2008; Revised Manuscript Received September 16, 2008

ABSTRACT: A group of triphenylamine-functionalized polyacetylenes (TPA-PAs) were synthesized using $[Rh(nbd)Cl]_2$ as catalyst in high yields (up to 93%). The polymers were characterized by NMR, IR, UV, PL, and CV analyses. The TPA pendants endowed the polymers with desirable redox activity and high photoconductivity. When an electron-withdrawing formyl group was attached to the TPA unit, the resultant polymer (P**3**) displayed solvatochromism. Simply mixing the polymers with multiwalled carbon nanotubes (MWNTs) in appropriate solvents resulted in the formation of TPA-PA/MWNT hybrids. With the aid of the polymer bearing styryl-TPA pendant (P**2**), ∼21% of MWNTs were loaded into the hybrid and a solubility of MWNTs in dichloromethane as high as 720 mg/L was achieved, which is among the highest solubilities of MWNTs in organic solvents. The great solvating power of the TPA-PAs for the MWNTs is attributed to the polymer wrapping processes aided by the additive effects of $\pi-\pi$ electronic interaction and donor−acceptor (D−A) complexation. This is the first report demonstrating the involvement of D−A interaction in the solubilization of MWNTs by a conjugated polymer. A single-layer photoreceptor with P**3**/MWNT hybrid as charge-generation material displayed a photosensitivity as high as ∼9091 $mm^2/mW \cdot s$, which is the highest value recorded for a polyacetylene-based device. The excellent photoconductivity is ascribed to the efficient charge separation in the D−A system and the fast transport of the photogenerated holes and electrons in the polymer and MWNT, respectively.

Introduction

Carbon nanotubes (CNTs) have attracted much interest among scientists and technologists because of their great scientific value and potential technological applications.[1] CNT-polymer hybridization has been under hot pursuit; as a result, much insight on the integration of CNTs with polymers have been gained.[2,3] Two issues, however, remain outstanding and require further research effort to understand: how to improve the dispensability of CNTs in organic solvents and how to choose appropriate polymer matrices with the ultimate goals of fabricating functional devices.

A few strategies have been developed to make CNTs miscible with common solvents,[4] among which the wrapping of CNTs in conjugated polymer chains is particularly attractive. As a representative route of noncovalent functionalization, this approach is harmless to the π-conjugation of CNTs and can thus preserve their unique and useful electronic and optical properties. In our previous studies, we solvated CNTs through noncovalent functionalization by poly(phenylacetylene) (PPA) and its pyrene-substituted derivatives.[5] PPA showed much higher solvating power to CNTs than its corresponding monomer due to the involved "polymer effect". The $\pi-\pi$ interaction between the pyrene pendants and the CNT walls made the polyacetylene chains prone to adhering onto the surfaces of the CNTs. The collective effects of the pendant/wall $\pi-\pi$ interaction and the polyacetylene chain wrapping conferred remarkably high CNT-solvating power on the pyrene-containing PPAs.[5]

PPA is a well-known conjugated polymer and its derivatives bearing appropriate substituents exhibit a variety of novel properties, including liquid crystallinity, light emission, photoconductivity, optical nonlinearity, chain helicity, self-assembly, biocompatibility, and cytophilicity.[6] The excellent solubility of the hybrids of the PPA derivatives and the CNTs with high CNT loadings in the common organic solvents has enabled the generation of processable materials with integrated advantageous attributes of the two components.[5]

Triphenylamine (TPA) is redox-active and hole-transporting and its derivatives have been widely used as hole-transport materials in the fabrication of organic light-emitting diodes.[7] It is envisioned that introduction of the TPA moiety into polyacetylene structure may lead to new polymers with novel and useful materials properties. Indeed, several TPA-containing polyacetylenes have been found to exhibit photoluminescence (PL), electrochromism, gas permeability, and chain helicity.[8,9] In this paper, we report our work on the synthesis of a group of novel TPA-functionalized polyacetylenes (TPA-PAs; Chart 1) and their hybridization with multiwalled carbon nanotubes

Chart 1

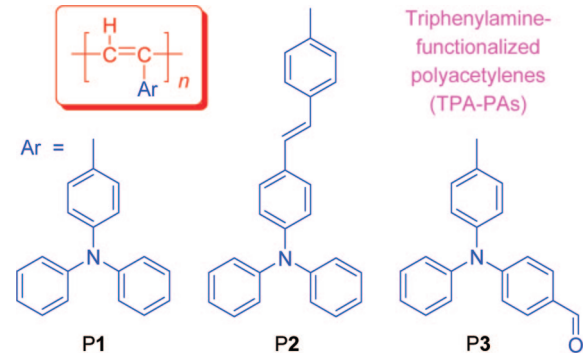

* To whom correspondence should be addressed. E-mail: sunjz@zju.edu.cn (J.Z.S.); tangbenz@ust.hk (B.Z.T.).
[†] Zhejiang University.
[‡] The Hong Kong University of Science and Technology.

10.1021/ma8014323 CCC: $40.75
Published on Web 10/29/2008

Scheme 1

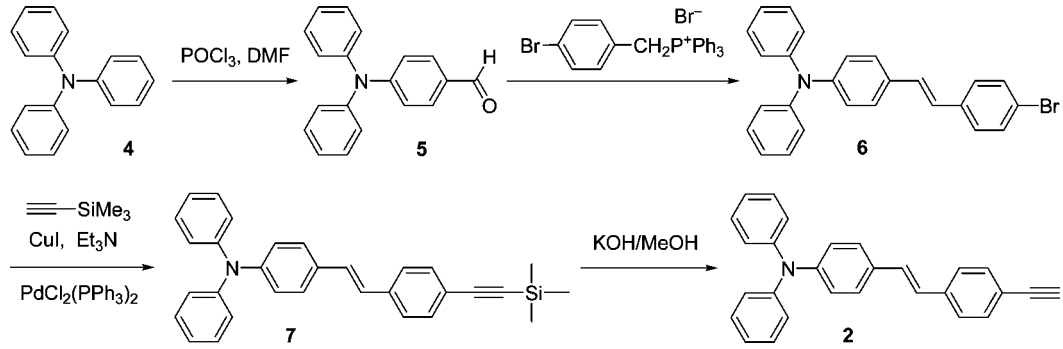

Scheme 2

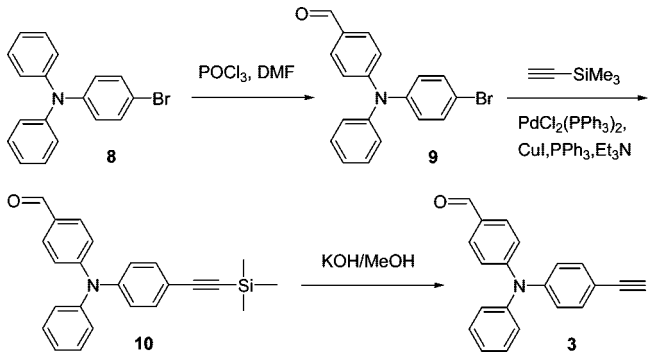

Table 1. Polymerizations of Triphenylamine-Functionalized Acetylene Monomers[a]

no.	monomer	$[M]_0$ (M)	[cat.][b] (mM)	yield (%)	M_w[c]	M_w/M_n[c]
1	**1**	0.250	10	89	83600	16.4
2	**2**	0.125	5	93	17600	4.9
3	**3**	0.125	5	49[d]	10200	4.4
4	**3**	0.050	2	26	12200	4.9
5	**3**	0.025	1	18	12000	4.3

[a] Carried out at room temperature under nitrogen for 24 h in THF/Et_3N. [b] Catalyst = $[Rh(nbd)Cl]_2$. [c] Estimated by gel permeation chromatograph (GPC) in THF on the basis of a polystyrene calibration. [d] Partially soluble in THF and DMSO.

(MWNTs) as well as their unique solvatochromism and high photoconductivity.

Results and Discussion

Polymer Synthesis. TPA-containing acetylene monomer **1** was prepared according to the published procedures (Scheme S1).[8a] The monomers with the TPA moiety functionalized by styryl (**2**) and formyl (**3**) groups were prepared by the multistep reactions shown in Schemes 1 and 2, respectively. Each step of the reactions proceeded smoothly and the desired acetylene monomers were obtained in good yields.

Monomers **1** and **2** were readily polymerized by $Rh(nbd)Cl]_2$ (nbd = 2,5-norbornadiene) in a mixture of THF (2 mL) and Et_3N (1 drop) and polymers P**1** and P**2** with high molecular weights were obtained in high yields (Table 1, nos. 1 and 2). The polymerization of monomer **3** was a challenge, because it contains a formyl group. The aldehyde moiety is active and may deactivate the catalyst. Luckily, P**3** was obtained in a moderate yield when $[Rh(nbd)Cl]_2$ and THF/Et_3N were used as catalyst and solvent, respectively. The product (P**3**) was, however, insoluble in dichloromethane (DCM), chloroform, and toluene and only partially soluble in tetrahydrofuran (THF) and dimethylsulfoxide (DMSO).

In our previous work, we found that the solubility of a pyrene-containing PPA was dependent on its molecular weight.[5b] When its molecular weight reached a critical value, the polymer became insoluble. To make P**3** completely soluble in common organic solvents, its molecular weight had to be controlled. When the concentrations of the monomer and catalyst were changed from 0.125 M and 5 mM to 0.05 M and 2 mM, respectively, the polymer yield was decreased to from 49% to 26% (cf., Table 1, nos. 3 and 4). The weight-average molecular weight (M_w) of the polymer was 12200 and it was completely soluble in common organic solvents. When the concentrations of the monomer and catalyst were further decreased to 0.025 M and 1 mM, respectively, the yield of the polymer was further decreased to 18%, although its M_w maintained virtually unchanged.

Structural Characterization. The polymeric products were characterized by spectroscopic methods, from which satisfactory analysis data were obtained (see Experimental Section for details). An example of the IR spectrum of P**3** is shown in Figure 1; the spectrum of its monomer **3** is also given in the same figure for the purpose of comparison. The monomer exhibits absorption bands at 3277 and 2097 cm^{-1} due to its ≡C−H and C≡C stretching vibrations, respectively. These absorption bands completely disappear in the spectrum of P**3**, indicating that the acetylenic triple bond of monomer **3** has been fully consumed by the polymerization reaction.

^1H NMR spectra of polymer P**3** and its monomer **3** are shown in Figure 2. As can be seen from the spectrum of P**3**, there is no resonance peak at δ 3.0, which is associated with the resonance of the acetylene proton of **3**. A new, weak peak associated with the resonance of olefinic proton appears at δ 5.8. The polymerization reaction transforms the acetylenic triple bond of **3** to the olefinic double bond of P**3**, which upfield-shifts the resonance of the phenyl protons, which now occurs in δ 6.4−7.8.

Figure 3 shows the ^{13}C NMR spectra of P**3** and its monomer **3**. Whereas the acetylenic carbon atom of **3** resonates at δ 84.4, this peak is completely absent in the spectrum of P**3**. Instead,

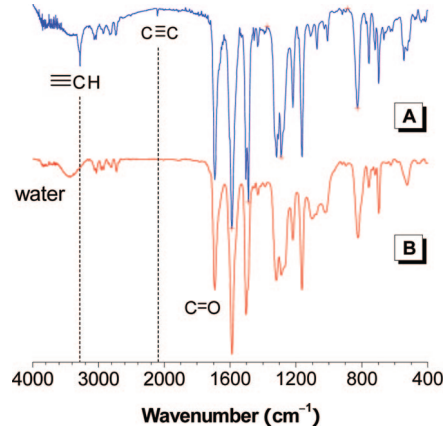

Figure 1. IR spectra of (**A**) monomer **3** and (B) its polymer P**3**.

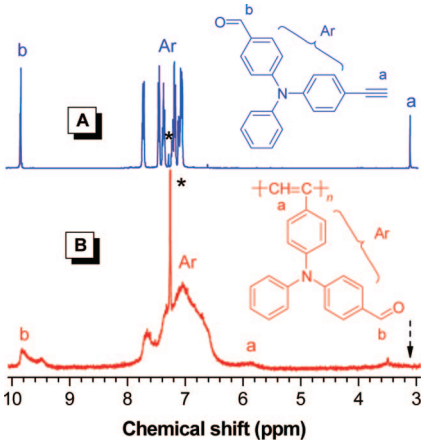

Figure 2. ^{1}H NMR spectra of (A) monomer **3** and (B) its polymer P**3** in chloroform-*d*. The solvent peaks are marked with asterisks.

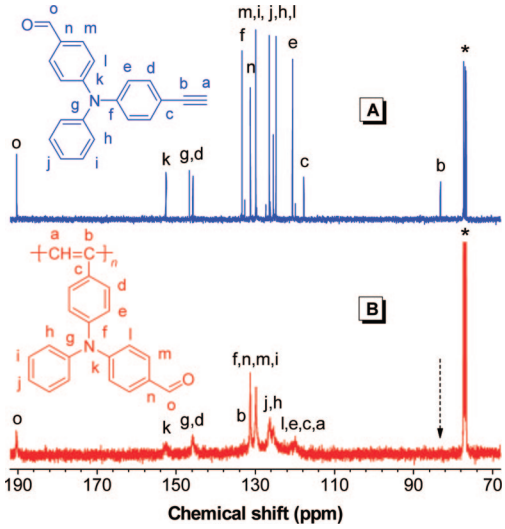

Figure 3. ^{13}C NMR spectra of (A) monomer **3** and (B) its polymer P**3** in chloroform-*d*. The solvent peaks are marked with asterisks.

two new weak peaks are observed at δ 133.6 and 116.1, which are assignable to the resonances of the carbon atoms of the polyene backbone. These spectral data once again prove that the polymerization has been realized by the transformation of the triple bond of the monomer to the double bond of the polymer.

Optical Properties of the Polymers. Absorption and emission spectra of polymers P**1**−P**3** are shown in Figure 4. The absorption peaks (λ_{ab}) at 308, 368, and 375 nm are due to $\pi-\pi^*$ electronic transitions of (substituted) TPA pendants in P**1**, P**3**, and P**2**, respectively. The red-shift in the λ_{ab} of the pendant is associated with the increase in its electronic conjugation. The polymers exhibit absorption band edges at longer wavelengths than their monomers (Supporting Information, Figure S1). Upon photoexcitation, the polymer solutions emit visible lights; the emission maximums (λ_{em}) of P**1**, P**2**, and P**3** appear at 437, 486, and 463 nm, with fluorescence quantum yields (Φ_F) of 4.5, 18.0, and 4.9%, respectively. These values are much lower than those of their corresponding monomers (Supporting Information, Figure S1) but are quite high in the family of PPA derivatives.[6,10]

Among the TPA-PAs, P**3** is unique. Its pendant of 4-(diphenylamino)benzaldehyde has a typical D-π-A structure, in which the diphenylamino, phenylene, and formyl groups function as donor, π-bridge, and acceptor, respectively. A D-π-A chromophore often shows solvatochromism. To check whether P**3**

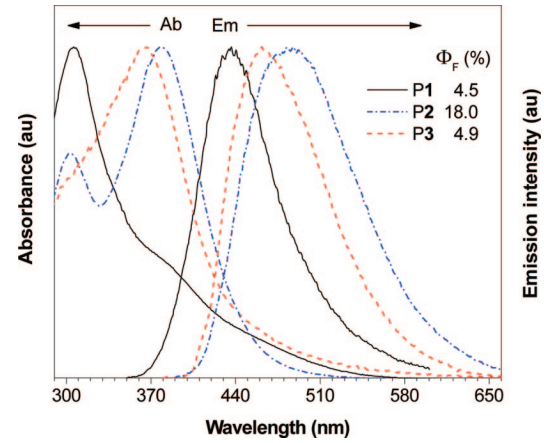

Figure 4. Absorption and emission spectra of TPA-PAs in THF. Concentration: ~10 μM. Excitation wavelength (nm): 308 (P**1**), 375 (P**2**), 368 (P**3**).

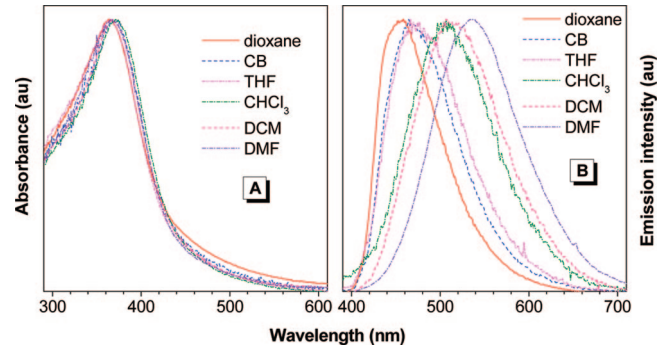

Figure 5. (A) Absorption and (B) emission spectra of P**3** in different solvents. Concentration: ~10 μM. Excitation wavelength: 368 nm.

Table 2. Photophysical Properties of P3 in Different Solvents[a]

solvent	Δf	λ_{ab} (nm)	λ_{em} (nm)	$\Delta\nu$ (cm^{-1})	Φ_F[b] (%)
dioxane	0.021	368.0	458.5	5310	10.7
CB	0.142	366.0	466.0	5863	9.5
chloroform	0.149	371.0	506.5	7211	2.6
THF	0.210	364.0	472.5	6306	4.8
DCM	0.218	365.0	506.5	7507	4.2
DMF	0.275	363.7	540.0	8801	1.6

[a] Abbreviations: CB = chlorobenzene, DMF = *N*,*N*-dimethylformamide, Δf = parameter of solvent polarity, λ_{ab} = absorption maximum, λ_{em} = emission maximum, and $\Delta\nu$ = Stokes shift. [b] Fluorescence quantum yield estimated using quinine sulfate in 0.1 N H_2SO_4 (Φ_F = 54%) as standard.

is solvatochromically active, its absorption and emission spectra were measured in solvents with different polarities. The absorption spectra of P**3** are similar, with virtually identical λ_{ab} values (~364−368 nm) recorded in different solvents (Figure 5A and Table 2). This indicates that the solvent polarity exerts little effect on its ground-state electronic transitions. In sharp contrast, the PL spectrum of P**3** bathochromically shifts with an increase in the solvent polarity (Figure 5B). Its λ_{em} shifts from 458.5 to 540.0 nm when the solvent is changed from dioxane to DMF. As displayed in Figure 6, the emission color changes from blue in dioxane to yellow in DMF when the polymer solutions are illuminated by a 365 nm UV lamp. The Φ_F value of polymer generally decreases with increasing polarity of the solvent, showing typical solvatochromic behavior or solvatokinetic effect.[11] The solvatochromism is caused by the photoinduced intramolecular charge transfer (CT) in the excited state.[12]

To further understand the solvent effects, the Stokes shifts of P**3** in different solvents were measured and the Lippert−Mataga

equation[13] was used to quantitatively describe its solvatochromic behavior:

$$\Delta\nu = \nu_{ab} - \nu_{em} = \frac{2\Delta f}{hca^3}(\mu_e - \mu_g)^2 + k \quad (1)$$

$$\Delta f = \frac{\varepsilon - 1}{2\varepsilon + 1} - \frac{n^2 - 1}{2n^2 + 1} \quad (2)$$

where $\Delta\nu$, h, c, a, ϵ, and n are the Stokes shift, the Planck constant, the speed of light, the radius of the chromophore, the dielectric constant, and the refractive index of the solvent, respectively, μ_e and μ_g are the dipolar moments in the excited (e) and ground (g) states, Δf is the solvent polarity parameter, and k is a constant. The linear dependence of $\Delta\nu$ on Δf together with the large slope of the $\Delta\nu$ versus Δf plot (Figure 7) suggests that the intramolecular CT excited-state has a larger dipolar moment than the ground-state due to the substantial charge redistribution, which is probably derived from the relaxation of the initially formed Franck−Condon excited state, instead of the direct transition from the ground state.[13]

Polymer/MWNT Hybridization. In our previous work, we found that polyacetylenes carrying π-conjugated pendants such as pyrene exhibited high solvating power to MWNTs.[5] The π-conjugated pendants play a key role in dispersing the bundles of MWNTs in the organic solvents. TPA is also π-conjugated and may thus enable the chains of the TPA-PAs to wrap onto the surfaces of the MWNTs, leading to good dispersion of MWNTs in organic solvents. This is indeed the case: the MWNTs are thickly wrapped by the macromolecular chains, as can be seen from Figure 8. The polymer layers in the **P1**/MWNT, **P2**/MWNT and **P3**/MWNT hybrids are about 100, 250, and 200 nm in thickness, respectively. The thick coating indicates good adherence of the polymers to the MWNTs.

The solubility of the MWNTs wrapped by **P3** is higher than that wrapped by **P1**, while the solubility of the MWNTs wrapped by **P2** is the highest among the three TPA-PAs (Figure 9). This trend can be ascribed to the electronic effect of the π-conjugated pendants, because the electronic conjugation in the pendants is **P2** > **P3** > **P1**. This conjugation-dependent solvating effect is consistent with our previous observations.[5] The solubility of the MWNTs hybridized with **P2** in DCM is as high as 720 mg/L, which is higher than the solubility of the CNTs hybridized with pyrene-functionalized PAs.[5] It is known that the π-conjugation in the planar pyrene ring is larger than that in the nonplanar TPA group. The remarkable solubility derived from **P2** thus cannot be simply explained by the conjugation effect of the pendants. In addition to the $\pi-\pi$ electronic interaction between the MWNT walls and the conjugated pendants, the donor−acceptor interaction may have played an important role in dispersing the MWNTs in the organic solvents.

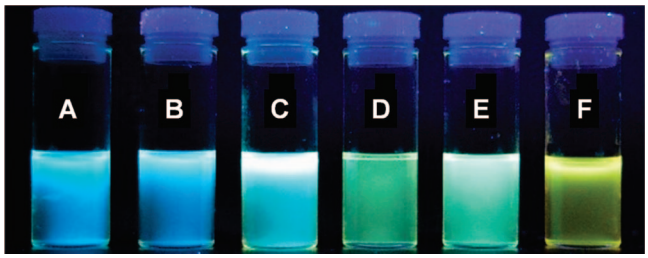

Figure 6. Photographs of **P3** solutions (~10 μM) in (A) 1,4-dioxane, (B) chlorobenzene, (C) THF, (D) chloroform, (E) DCM, and (F) DMF taken under illumination of a 365 nm UV lamp.

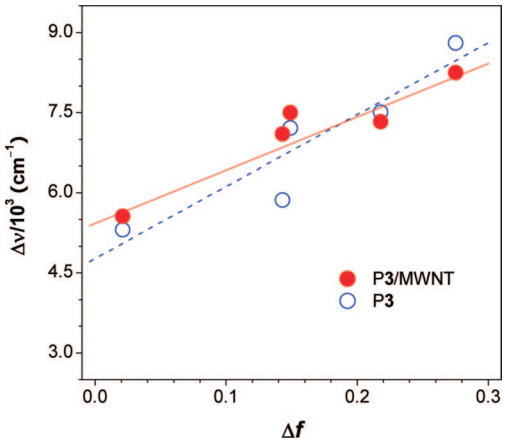

Figure 7. Plots of Stokes shift ($\Delta\nu$) of (A) **P3** and (B) **P3**/MWNT versus solvent polarity parameter (Δf).

Optical Properties of the Hybrids. The wrapping of the polymer chains onto the MWNT walls bestows the hybrids with not only desirable solubility but also new functionality. TPA is a fluorescent chromophore, which confers light-emitting capability on the TPA-PA/MWNT hybrids. The Φ_F values of the **P1**/MWNT, **P2**/MWNT and **P3**/MWNT hybrids in THF are 1.5, 16.0, and 4.6%, respectively, which are somewhat lower than those of their parent polymers (cf., Figure 4), suggestive of energy and charge transfers between the fluorophores and the MWNTs.

The absorption and emission spectra of the **P3**/MWNT hybrid in the solvents with different polarities are shown in the upper panel of Figure 10. The photographs given in the lower panel of the figure presents a direct evidence for the solvatochromism in the hybrid. However, from the comparison with Figures 5 and 10, one can see that the solvatochromic effect of the hybrid is weaker than that of its parent polymer **P3**. For **P3**, its emission peak shift from 458.5 to 540.0 nm when the solvent is changed from dioxane to DMF, whereas for **P3**/MWNT, its λ_{em} value changes from 460.0 to 527.0 nm with the same variation in the solvent polarity. The Lippert-Mataga plots provide a quantitative comparison: the slope of the plot for **P3** is larger than that for **P3**/MWNT (cf., Figure 7), indicating that the excited-state of the polymer has a larger dipolar moment than that of the hybrid. As a result, the former exhibits stronger solvatochromism than the latter.

The difference in the dipolar moments between the excited chromophores in **P3** and **P3**/MWNT is resulted from the interaction between the polymer chains and the MWNT walls. The MWNTs are electron-accepting, which competes with the D−A interaction between the amino donor and the formyl acceptor (Chart 2). Without the interaction with the MWNT walls, the 4-(diphenylamino)benzaldehyde pendant in **P3** is a typical D-π-A structure and exhibits pronounced solvatochromism. When **P3** is hybridized with the MWNTs, the TPA moiety partly donates its charge to the MWNTs. The electron-donating effect of the amino unit becomes weaker, as a consequence of which, the solvatochromism of the **P3**/MWNT hybrid becomes weaker than that of its parent polymer **P3**.

The above mechanism is based on the assumption that the MWNTs act as an acceptor, which causes the intermolecular charge transfer from TPA to MWNTs. To verify this assumption, we investigated the solvatochromism of **P1** and **P1**/MWNTs. **P1** shows a weak solvatochromic effect because it is not a D-π-A structure (Figure 11A). An evident solvatochromism, however, is observed in the **P1**/MWNT hybrid (Figure 11B). The PL spectrum of the **P1**/MWNT hybrid progressively shifts to red with an increase in the solvent polarity: its λ_{em} shifts from 434.0 to 500.0 nm when the solvent is changed from dioxane to DMF. The slope of the Lippert−Mataga plot for **P1**/MWNTs is larger than that for **P1** (Figure 12), indicative of a larger dipolar moment of excited-state of the

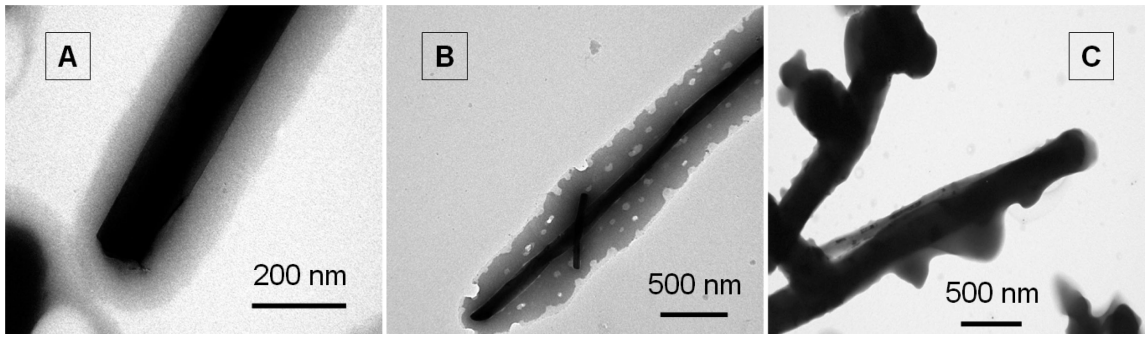

Figure 8. TEM images of the hybrids of TPA-PAs and MWNTs: (A) P**1**/MWNTs, (B) P**2**/MWNTs, and (C) P**3**/MWNTs.

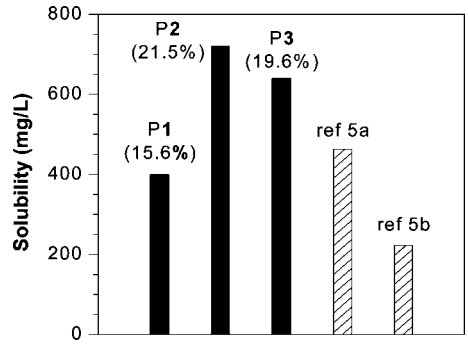

Figure 9. Solubility of TPA-PA/WMNT hybrids in DCM. The contents of MWNTs in the hybrids given in parentheses (in %) were calculated according to the method reported in ref 5b. The data for the CNTs wrapped by the pyrene-containing PAs[5b] are shown for comparison.

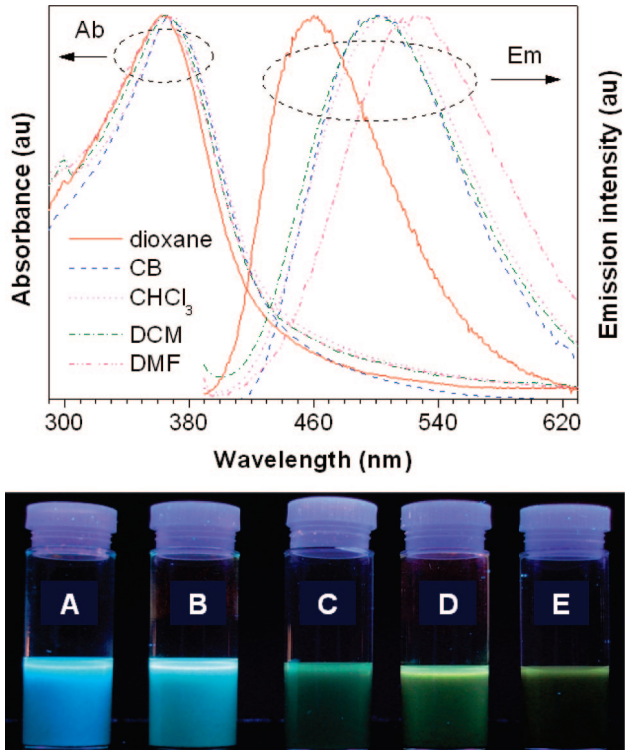

Figure 10. (Upper panel) Absorption and emission spectra of P**3**/MWNT hybrid in different solvents. Concentration: ~10 μg/mL. Excitation wavelength: 368 nm. (Lower panel) Photographs of P**3**/MWNT hybrid solutions (~0.1 mg/mL) in (A) 1,4-dioxane, (B) CB, (C) chloroform, (D) DCM, and (E) DMF taken under illumination of a 365 nm UV lamp.

hybrid than its parent polymer. Similar results were obtained for P**2** and P**2**/MWNTs: the former shows weaker solvatochromic effect than the latter (Supporting Information, Figure S2). These results confirm that the MWNTs behave as an electron acceptor.

Redox Activity. The TPA group is redox active[8,9,14] and thereby it is reasonable to conceive that the TPA-PAs and their hybrids with MWNTs are also redox active. The electrochemical behaviors of the polymers and hybrids were investigated in DCM solutions. P**3** shows one set of single redox wave and the related $E_{1/2}$ and ΔE_P values are 562 and 315 mV, respectively (Figure 13). The single peak indicates that there is no electronic crosstalk between the TPA moieties. The P**3**/MWNT hybrid shows similar redox behavior, but its $E_{1/2}$ and ΔE_P values are much higher, being 986 and 559 mV, respectively. The pronounced change in the oxidation potential confirms the strong electronic interaction between TPA and MWNTs. Similarly high ΔE_P values are obtained in the P**1**/MWNT and P**2**/MWNT hybrid systems (Supporting Information, Figure S3). The electrochemical data are in agreement with the observations of enhanced solubility, thick polymer coating on the MWNT surface, and the strong solvatochromism.

Photoconduction. Much work has been done on the photoconduction in substituted polyacetylenes.[6] It has been found that (i) the polyacetylenes containing electron-donating substituents exhibit higher photoconductivity (PC) than those with electron-accepting ones, (ii) the PC is further improved when the donor substituents are simultaneously good hole-transporters, and (iii) the photoconduction becomes more efficient when the donor substituents are mesogenic and can be packed in an ordered fashion.[15] TPA is a typical donor and a famous building block for hole-transport materials.[7] The TPA-PAs are thus anticipated to show good photoconduction performances.

To verify this expectation, single-layered photoreceptors were fabricated using the TPA-PAs and their MWNT hybrids as chare-generation materials (CGMs) and the PC values of the devices were measured with a standard GDT-II photoinduced discharge instrument.[15−17] Upon exposure to the illumination of a white light, the initial surface potential (V_i) of the device drops. For the photoreceptor with P**1** as CGM, the V_i value swiftly plummets to a very low residual surface potential (V_r = 18 V) after the photoinduced discharge (Table 3, no. 1). The half-discharge time ($T_{1/2}$) of P**3** is 0.09 s and the photosensitivity (S) is 1010.1 mm^2/mW·s, which is quite high among substituted polyacetylenes.[6,15,18]

The photoreceptor with P**3** as CGM shows a lower S value than the device based on P**1**. This is easy to understand because the formyl group attached to the TPA moiety is electron-withdrawing, which decreases the hole-transport efficiency. The photoreceptor with P**2** as CGM gives the lowest S value among the TPA-PAs. This result can be explained in terms of charge generation efficiency. P**2** has the highest fluorescence quantum efficiency among the polymers. This indicates that the photogenerated geminate pairs have a high probability to recombine. Consequently, the number of the photogenerated free charges

Chart 2

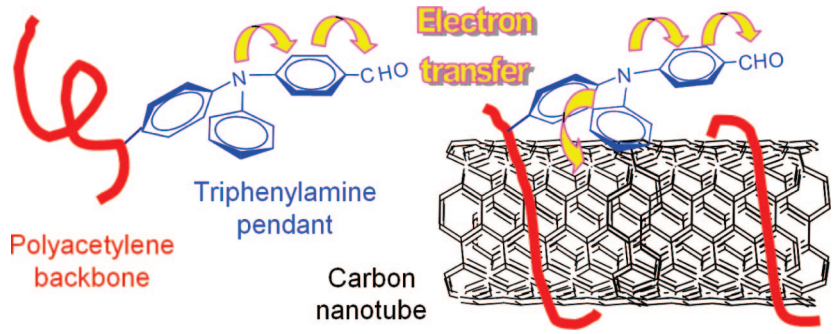

in the P**2**-based photoreceptor becomes smaller and its PC thus becomes lower.

All the photoreceptors fabricated with the hybrids as CGMs displayed improved PCs in comparison to the parent polymer-based devices. Amazingly, the P**3**/MWNT-based photoreceptor shows a $T_{1/2}$ value as low as 0.01 s. Its corresponding S value is as high as ~9091 mm^2/mW·s, about 40 times that of the P**3**-based device. This dramatically enhanced PC is due to the MWNT component in the photoreceptor. As discussed above, the MWNTs behave as an electron acceptor. The existence of the MWNTs in the charge-generation layer improves charge-generation efficiency through a mechanism of photoinduced charge transfer from P**3** to MWNTs. Meanwhile, the MWNTs offer one-dimensional electron-transport channels. Their conductive networks quickly transport the photogenerated electrons to the surface of the photoreceptor to neutralize the surface charge, thus resulting in steeply decreased surface potential and transiently short $T_{1/2}$ value. The device with P**1**/MWNT hybrid as CGM also shows enhanced PC but the enhancement is less

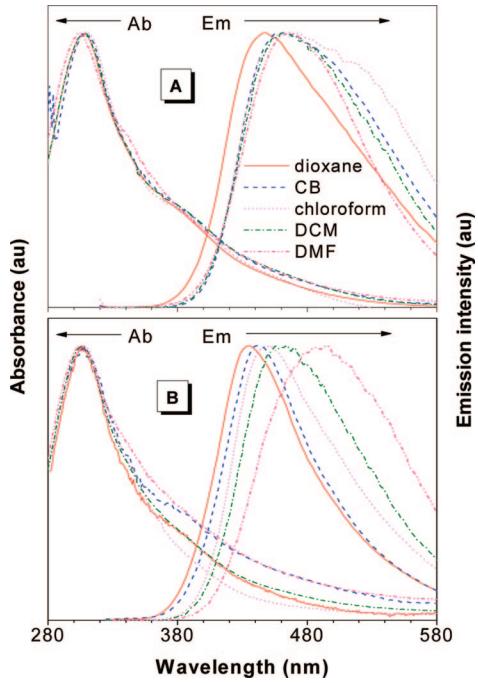

Figure 11. Absorption and emission spectra of (A) P**1** and (B) P**1**/MWNT in different solvents. Concentration: ~10 μM. Excitation wavelength: 308 nm.

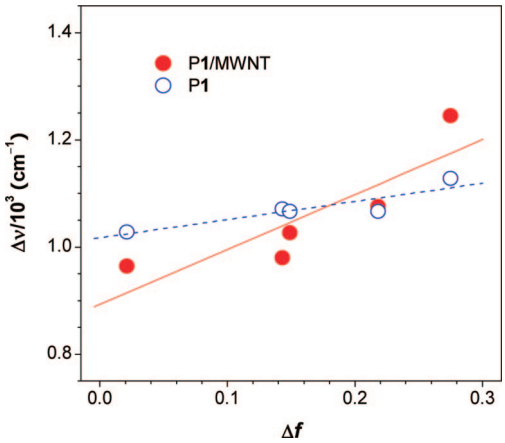

Figure 12. Plot of Stokes shift ($\Delta\nu$) of (A) P**1** and (B) P**1**/MWNT versus solvent polarity parameter (Δf).

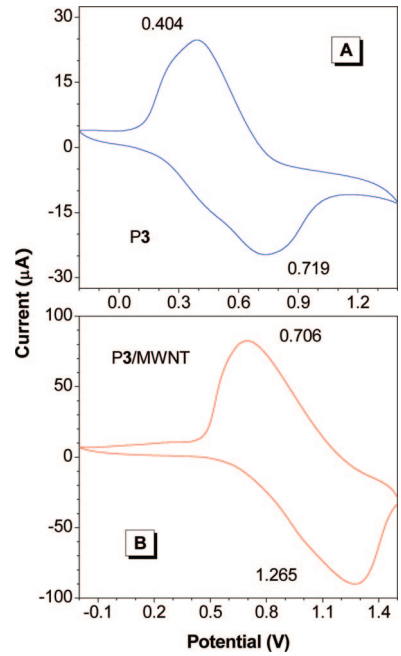

Figure 13. Cyclic voltammograms of (A) P**3** and (B) P**3**/MWNT measured in DCM containing 0.2 M Bu_4NClO_4 at a scan rate of 50 mV/s.

Table 3. Photoconductions in TPA-PAs and their MWNT Hybrids[a]

no.	CGM	V_i (V)	V_r (V)	$T_{1/2}$ (s)	S (mm^2/mW·s)
1	P**1**	538	18	0.09	1010.1
2	P**1**/MWNT	622	65	0.02	4545.5
3	P**2**	841	35	0.51	178.3
4	P**2**/MWNT	591	24.5	0.18	505.1
5	P**3**	742	41	0.40	227.3
6	P**3**/MWNT	769	11	0.01	9090.9

[a] Measured in single-layer photoreceptors. Abbreviations: CGM = charge-generation material, V_i = initial surface potential, V_r = residual potential after photoinduced discharge, $T_{1/2}$ = half-discharge time, and S = photosensitivity.

than that for the P**3**/MWNT-based device. This is because P**1** has a relative low capacity of loading MWNTs into its hybrid, which leads to a less efficient charge separation and transportation.

Concluding Remarks. In this work, we have prepared a group of TPA-functionalized acetylene monomers and investigated their polymerization behaviors. The organorhodium complex $[Rh(nbd)Cl]_2$ efficiently catalyzed the polymerizations of the acetylene monomers, including the monomer with formyl functional group (**3**). The resultant TPA-PAs are soluble, fluorescent, solvatochromic, redox-active, and photoconductive.

The TPA-PAs exhibited great solvating power to the MWNTs. For example, simply mixing P**2** with the MWNTs gave the P**2**/MWNT hybrids with up to ~21 wt % of MWNT loading. With the aid of the wrapped polymer chains, the solubility of the MWNTs reached 720 mg/L in DCM, which ranks among the highest solubilities of the CNTs recorded for conjugated polymer/CNT hybrids. The capability of π-conjugated polymers to help dissolve MWNTs is usually ascribed to the $\pi-\pi$ interactions between the polymers and the MWNTs. In our previous work, we observed an additive effect, in which the polymer chain wrapping around the MWNT surfaces and the conjugated pendant/MWNT wall interactions were found to work synergistically to realize the MWNT dissolution in common organic solvents.[5] In this work, a new effect, that is, D−A complexation, was found to play a role in the MWNT dissolution process. This observation offers a new strategy for the design and fabrication of macroscopically processable polymer/CNT hybrids.

The strong D−A interactions between TPA-PAs and MWNTs were confirmed by the electrochemical and photophysical investigations. The $E_{1/2}$ values of P**3** and P**3**/MWNT appeared at 512 and 986 mV, respectively. The pronounced change in the oxidation potential presented a direct evidence for the strong electronic interaction between the TPA moiety and the MWNT wall. P**3** exhibited very strong solvatochromism. Its PL spectrum bathochromically shifted with an increase in the dipolar moment of solvent. The red-shift in the PL spectrum of the P**3**/MWNT hybrid with solvent was decreased in extent, because the D−A interactions between the TPA moiety and the MWNT wall had weakened the electron-donating capability of the amino group and hence the photoinduced intramolecular charge transfer.

The photoreceptor with P**3**/MWNT as CGM gave an S value as high as 9090.9 $mm^2/mW\cdot s$, which is unprecedented for polyacetylene-based devices.[6,18] The excellent PC in the hybrid-based photoreceptor is probably due to the efficient photoinduced charge separation in the D−A system and the fast transport of the photogenerated electrons in the MWNT networks. The unique and useful properties described above make the hybrids promising to find technological applications as advanced functional materials.

Experimental Section

Materials. THF (Labscan), toluene (BDH), and 1,4-dioxane (Aldrich) were distilled from sodium benzophenone ketyl under nitrogen immediately prior to use. DMF was stirred over calcium hydride overnight, distilled under reduced pressure, and stored in an atmosphere of nitrogen. Other solvents were purified by standard procedures. Dichlorobis(triphenylosphine)palladium(II), triphenylphosphine, copper(I) iodide, and other reagents and solvents were all purchased from Aldrich and used as received without further purification. $[Rh(nbd)Cl]_2$ was prepared according to the published procedures.[19]

Instrumentations. The ^1H and ^{13}C NMR spectra were measured on a Mercury plus 300 MHz NMR spectrometer using tetramethylsilane (TMS; $\delta = 0$ ppm) as internal standard. The IR spectra were recorded on a Bruker VECTOR 22 spectrometer and the UV−vis absorption spectra were taken on a Varian CARY 100 Bio spectrophotometer. The mass spectra were measured on a GCT Premier CAB 048 mass spectrometer and the elemental analysis was performed on an Eager 300 microanalyzer. The PL spectra were measured on a Hitachi 4500 fluorescence spectrophotometer and the Φ_F values were estimated using quinine sulfate in 0.1 N sulfuric acid ($\Phi_F = 54\%$) as standard. The absorbance of the solution was kept below 0.1 to avoid internal filter effect.

The average molecular weights (M_w and M_n) and polydispersity indexes (PDIs) of the polymers were estimated by a Waters Associates GPC system in THF. A set of monodisperse polystyrene standards covering molecular weight range of 10^3-10^7 was used for the molecular weight calibration. The thermogravimetric analysis (TGA) was conducted on a Pyris 6 thermogravimetric analyzer (Perkin-Elmer), in which a sample of ~3 mg was heated to 800 °C at a rate of 10 °C/min under a flow of nitrogen stream (Supporting Information, Figure S4). The TEM images were obtained on a JEM-200CX microscope.

Monomer Synthesis. Monomer **1** was prepared according to the published procedures.[8a] IR (KBr, ν, cm^{-1}): 3272 (HC≡C), 2100 (C≡C). ^1H NMR (300 MHz, $CDCl_3$, δ, TMS, ppm): 3.01 (s, 1H), 6.93 (m, 2H), 7.05 (m, 6H, Ar), 7.31 (m, 6H, Ar). ^{13}C NMR ($CDCl_3$): 75.9, 83.8, 114.7, 121.8, 123.4, 124.7, 129.2, 132.8, 146.8, 148.1. HRMS (MALDI-TOF, *m/z*): calcd, 269.1204; found, 269.1205 (M^+).

Monomers **2** and **3** were prepared according to the synthetic routes shown in Schemes 1 and 2. The detailed experimental procedures are given below.

*Preparation of 4-(Diphenylamino)benzaldehyde (**5**).* This compound was prepared by the Vilsmeier−Haack formylation reaction.[20] ^1H NMR (300 MHz, $CDCl_3$, δ, TMS, ppm): 9.81 (s, 1H), 7.66 (d, 2H), 7.34 (t, 4H), 7.19 (m, 6H), 7.00 (d, 2H).

*Preparation of (E)-4-(4-Bromostyryl)-N,N-diphenylaniline (**6**).* Compound **5** (1.9 g, 7.2 mmol), Wittig reagent (5.6 g, 10.8 mmol), which was prepared from 1-bromo-4-(bromomethyl)benzene and triphenylphosphine in DMF, and a catalytic amount of 18-crown-6 were dissolved in 100 mL of DMF under nitrogen. The mixture was cooled to 0−5 °C with an ice bath, to which 2.8 g of potassium *t*-butoxide (25 mmol) was added. The mixture was stirred under nitrogen at room temperature for 2 days and then poured into a large amount of water (700 mL). The precipitate was collected and purified by a silica gel column using hexane as eluent. A yellow solid was obtained in 59% yield (1.8 g). ^1H NMR (300 MHz, $CDCl_3$, δ, TMS, ppm): 7.48 (m, 6H), 7.3 (m, 4H), 7.27 (m, 4H), 7.13 (m, 6H).

*Preparation of (E)-N,N-Diphenyl-4-{4-[2-(trimethylsilyl)ethynyl]-styryl}aniline (**7**).* A 300 mL three-necked flask was equipped with a three-way stopcock and a magnetic stirring bar and flushed with dry nitrogen. Compound **6** (1.8 g, 4.2 mmol), (trimethylsilyl)acetylene (2.1 mL, 4.5 mmol), cuprous iodide (40 mg, 21 mmol), triethylamine (50 mL), piperidine (10 mL), triphenylphosphine (40 mg, 0.17 mmol), and dichlorobis(triphenylosphine)palladium(II) (40 mg, 0.084 mmol) were fed into the flask. The mixture was stirred at room temperature overnight, after which, triethylamine and piperidine were evaporated off and diethyl ether (50 mL) was added to dissolve the residue. Insoluble salt was filtered off and the filtrate was concentrated with a rotary evaporator. The crude product was purified by flash silica gel column chromatography using a mixture of petroleum ether and ethyl acetate (5:1 by volume) as eluent. A yellow solid of **7** was obtained in 40% yield. ^1H NMR (300 MHz, $CDCl_3$, δ, TMS, ppm): 7.50 (m, 5H), 7.42 (d, 2H), 7.30 (s, 1H), 7.14 (d, 5H), 7.12 (d, 5H), 6.97 (d, 2H), 0.24 (s, 9 H).

Synthesis of (E)-4-(4-Ethynylstyryl)-N,N-diphenylaniline (Monomer 2). Compound **7** (0.74 g, 1.7 mmol), methanol (200 mL), and KOH (0.56 g, 10 mmol) were placed in a round-bottomed flask equipped with a septum and a stirring bar. The mixture was stirred at room temperature for 8 h and then poured into 1000 mL of 1 M HCl solution. The mixture was extracted by DCM three times and the organic layers were combined. After the solvent was removed under reduced pressure, the crude product was purified by silica gel column using a mixture of petroleum ether and ethyl acetate (5:1

v/v) as eluent. A yellow solid was obtained in 95% yield. IR (KBr, ν, cm^{-1}): 3280 (HC≡C), 2107 (C≡C). ^1H NMR (300 MHz, $CDCl_3$, δ, TMS, ppm): 7.50 (m, 5H), 7.42 (d, 2H), 7.31 (s, 1H), 7.15 (d, 5H), 7.13 (d, 5H), 7.00 (d, 2H), 3.14 (s, 1H). ^{13}C NMR (75 MHz, $CDCl_3$, δ, TMS, ppm): 152.6, 146.5, 145.6, 133.3, 132.5, 131.2, 129.7, 129.4, 127.1, 126.2, 125.1, 124.6, 120.5, 119.7, 117.5, 83.0. Anal. Calcd for $C_{28}H_{21}N$ (371.47): C, 90.53; H, 5.70; N, 3.77. Found: C, 90.39; H, 5.72; N, 3.82. Mass (*m*/*z*): 371.17 (M^+).

*Preparation of 4-[N-(4-Bromophenyl)-N-phenylamino]benzaldehyde (**9**).* This intermediate was prepared from **8** by a procedure similar to that used for the preparation of **5**. A yellow solid was obtained in 90.5% yield. ^1H NMR (300 MHz, $CDCl_3$, δ, TMS, ppm): 9.84 (s, 1H), 7.70 (d, 2H), 7.44 (d, 2H), 7.36 (m, 3H), 7.20−7.00 (m, 6H).

*Preparation of 4-(N-{4-[2-(Trimethylsilyl)ethynyl]phenyl}-N-phenylamino)benzaldehyde (**10**).* This compound was prepared by the Sonogashira coupling reaction similar to that used for the preparation of **7**. A yellow liquid was obtained in 72% yield. ^1H NMR (300 MHz, $CDCl_3$, δ, TMS, ppm): 9.81 (s, 1H), 7.70 (d, 2H), 7.44 (m, 5H), 7.21−7.00 (m, 6H), 0.24 (s, 9H).

*Synthesis of 4-[N-(4-Ethynylphenyl)-N-phenylamino]benzaldehyde (Monomer **3**).* The monomer was prepared by the procedures similar to those used for the prepared of **2**. A yellow solid was obtained in 98% yield. IR (KBr, ν, cm^{-1}): 3282 (HC≡C), 2104 (C≡C), 1588 (C═O). ^1H NMR (300 MHz, $CDCl_3$, δ, TMS, ppm): 9.81 (s, 1H), 7.71 (d, 2H), 7.44 (d, 2H), 7.35 (m, 3H), 7.19 (m, 4H), 7.00 (d, 2H), 3.06 (s, 1H). ^{13}C NMR δ (ppm): 190.4, 152.8, 146.8, 145.6, 133.3, 131.5, 130.0, 129.8, 126.5, 125.5, 124.8, 120.6, 117.8, 83.3, 77.3. Anal. Calcd for $C_{21}H_{15}NO$ (297.35): C, 84.82; H, 5.08; N, 4.71. Found: C, 84.51; H, 5.17; N, 4.33. Mass (*m*/*z*): 297.12 (M^+).

Polymerization Reactions. Monomers **1**−**3** were polymerized under dry nitrogen using the Schlenk techniques in a vacuum-line system. Typical experimental procedures for the polymerization of **1** are given below as an example.

Into a baked 20 mL Schlenk tube with a sidearm was added 160 mg (0.5 mmol) of monomer **1**. The tube was evacuated under vacuum and flushed with dry nitrogen three times through the sidearm. THF (1 mL) was then injected into the tube to dissolve the monomer. The catalyst solution was prepared in another tube by dissolving 4.6 mg of $[Rh(nbd)Cl]_2$ in 1 mL of a THF/Et_3N mixture, which was transferred to the monomer solution using a hypodermic syringe. The mixture was stirred at room temperature under nitrogen for 24 h and was then diluted with 6 mL of THF and added dropwise to 500 mL methanol through a cotton filter under stirring. The precipitate was allowed to stand for 24 h and then filtered with a Gooch crucible. The polymer was washed with methanol five times and dried in a vacuum oven at 40 °C to a constant weight.

*Characterization Data for P**1**.* Red powdery solid; yield 89.0% (Table 1, no. 1). M_w, 83600; M_w/M_n, 16.4. IR (KBr, ν, cm^{-1}): 3061, 3032, 1589−692. ^1H NMR (300 MHz, $CDCl_3$, δ, TMS, ppm): 7.9−5.8 (broad, m). ^{13}C NMR (75 MHz, $CDCl_3$, δ, TMS, ppm): 148.0, 146.8, 136.2, 132.6, 129.1, 124.6, 123.2, 121.8, 116.1, 114.1.

*P**2**.* Yellow solid; yield 93.0% (Table 1, no. 2). M_w, 17600; M_w/M_n, 4.9. IR (KBr, ν, cm^{-1}): 3028, 1590−693. ^1H NMR (300 MHz, $CDCl_3$, δ, TMS, ppm): 7.5−6.0 (broad, m). ^{13}C NMR (75 MHz, $CDCl_3$, δ, TMS, ppm): 155.5, 147.7, 147.5, 136.5, 132.1, 129.1, 128.1, 127.4, 127.2, 127.0, 126.2, 125.1, 124.6, 121.0, 119.9, 117.1.

*P**3**.* Yellow solid; yield 26.0% (Table 1, no. 4). M_w, 12200; M_w/M_n, 4.9. IR (KBr, ν, cm^{-1}): 3282, 2948, 2798, 2718, 1692, 1586−691. ^1H NMR (300 MHz, $CDCl_3$, δ, TMS, ppm): 9.8, 7.8−5.8 (broad). ^{13}C NMR (75 MHz, $CDCl_3$, δ, TMS, ppm): 153.1, 146.1, 145.5, 132.3, 131.4, 131.2, 130.7, 129.9, 126.4, 125.6, 125.1, 122.5, 120.8, 119.9, 116.1.

Polymer/Nanotube Hybridization. The preparation of P**3**/MWNT hybrid is described below as an example: into a tube with a stir bar were added 10 mg of P**3**, 10 mg of MWNTs, and 5 mL of DCM. After stirring for half an hour, the mixture was filtered through a cotton filter to remove the insoluble MWNTs. The filter was heated in an oven at 120 °C to a constant weight. The concentration of the MWNTs in DCM was calculated using our previously published method.[5b]

Electrochemical Measurement. The cyclic voltammograms were recorded on a Princeton Applied Research 273A potentiostat. The working and reference electrodes were glassy carbon and Ag/AgCl, respectively. Potentials were reported with reference to a ferrocenium-ferrocene pair ($Cp_2Fe^{+/0}$). The scan rate was set at 50 mV/s and the concentration of the supporting electrolyte Bu_4NClO_4 was 0.2 M.

PC Measurement. Photoconduction parameters of the single-layered photoreceptors were evaluated with a standard GDT-II photoinduced discharge instrument.[16] The surface of the photoreceptor was first negatively corona-charged to a surface potential of V_0. After dark discharge for 3 s with the surface potential dropped to V_i, the photoreceptor was exposed to a white light with an intensity (I) of 0.011 mW/mm^2. Electron−hole pairs were generated upon exposure to the light source. The charge pairs disassociated to give rise to free carriers with the aid of an external field and the holes migrated toward the negatively charged surface following the applied field through the conductive channels provided by the charge-transport material. The surface charge was neutralized with a V_r left. From the discharge experiment, the half-discharge exposure energy was determined by the equation of $E_{1/2} = t_{1/2}I$, where $t_{1/2}$ is the half-discharge time or the time needed for the initial potential V_i to decay to its half-value under exposure to the light source. Photosensitivity S is defined as the reciprocal of $E_{1/2}$, that is, $S = 1/E_{1/2}$.

Acknowledgment. This work was partially supported by the National Science Foundation of China (Project Nos. 20634020, 50573065, and 50740460164), the Research Grants Council of Hong Kong (603008, 602707, and 602706), and the Ministry of Science and Technology of China (2009CB623600). B.Z.T. thanks the support from the Cao Guangbiao Foundation of Zhejiang University.

Supporting Information Available: Synthetic scheme for the preparation of monomer **1**, absorption and emission spectra of monomers **1**−**3** in THF, and P**2** and P**2**/MWNT in different solvents, cyclic voltammograms of P**1**, P**2** and their MWNT hybrids, and TGA thermograms of P**1**−P**3**. This material is available free of charge via the Internet at http://pubs.acs.org.

References and Notes

(1) (a) Baughman, R. H.; Cui, C. X.; Zakhidov, A. A.; Iqbal, Z.; Barisci, J. N.; Spinks, G. M.; Wallace, G. G.; Mazzoldi, A.; De Rossi, D.; Rinzler, A. G.; Jaschinski, O.; Roth, S.; Kertesz, M. *Science* **1999**, *284*, 1340. (b) Ajayan, P. M.; Terrones, M.; de la Guardia, A.; Huc, V.; Grobert, N.; Wei, B. Q.; Lezec, H.; Ramanath, G.; Ebbesen, T. W. *Science* **2002**, *296*, 705. (c) Fennimore, A. M.; Yuzvinsky, T. D.; Han, W.-Q. M.; Fuhrer, S.; Cumings, J.; Zettl, A. *Nature* **2003**, *424*, 408. (d) Samit, V. A.; Terentjev, E. M. *Nat. Mater.* **2005**, *4*, 491. (e) Kam, N. W. S.; O'Connell, M.; Wisdom, J. A.; Dai, H. L. *Proc. Natl. Acad. Sci. U.S.A.* **2005**, *102*, 11600.

(2) (a) Lin, Y.; Meziani, J. M.; Sun, Y.-P. *J. Mater. Chem.* **2007**, *17*, 1143. (c) Li, C.; Thostenson, E. T.; Chou, T. W. *Compos. Sci. Technol.* **2008**, *68*, 1227. (d) Cicoira, F.; Santato, C. *Adv. Funct. Mater.* **2007**, *17*, 3421.

(3) (a) Tasis, D.; Tagmatarchis, N.; Bianco, A.; Prato, M. *Chem. Rev.* **2006**, *106*, 1105. (b) Kauffman, D. R.; Star, A. *Chem. Soc. Rev.* **2008**, *37*, 1197. (c) Kilina, S.; Tretiak, S. *Adv. Funct. Mater.* **2007**, *17*, 3405.

(4) (a) Chen, Y.; Lin, Y.; Liu, Y.; Doyle, J.; He, N.; Zhuang, X. D.; Bai, J. R.; Blau, W. J. *J. Nanosci. Nanotechnol.* **2007**, *7*, 1268. (b) Murakami, H.; Nakashima, N. *J. Nanosci. Nanotechnol.* **2006**, *6*, 16. (c) Fu, K. F.; Sun, Y. P. *J. Nanosci. Nanotechnol.* **2003**, *3*, 351. (d) Dyke, C. A.; Tour, J. M *J. Phys. Chem. A* **2004**, *108*, 11151. (e) Shen, J. F.; Hu, Y. Z.; Qin, C.; Ye, M. X. *Langmuir* **2008**, *24*, 3993.

(5) (a) Tang, B. Z.; Xu, H. *Macromolecules* **1999**, *32*, 2569. (b) Yuan, W. Z.; Sun, J. Z.; Dong, Y. Q.; Häuβler, M.; Yang, F.; Xu, H. P.; Qin, A. J.; Lam, J. W. Y.; Zheng, Q.; Tang, B. Z. *Macromolecules* **2006**, *39*, 8011. (c) Yuan, W. Z.; Mao, Y.; Zhao, H.; Sun, J. Z.; Xu, H. P.; Jin, J. K.; Zheng, Q.; Tang, B. Z. *Macromolecules* **2008**, *41*, 701. (d) Yuan, W. Z.; Sun, J. Z.; Liu, J. Z.; Dong, Y.; Li, Z.; Xu, H. P.; Qin, A. J.; Haussler, M.; Jin, J. K.; Zheng, Q.; Tang, B. Z. *J. Phys. Chem. B* **2008**, *112*, 8896.

(6) (a) Lam, J. W. Y.; Tang, B. Z. *J. Polym. Sci., Part A: Polym. Chem.* **2003**, *41*, 2607. (b) Lam, J. W. Y.; Tang, B. Z. *Acc. Chem. Res.* **2005**, *38*, 745. (c) Li, Z.; Dong, Y.; Qin, A.; Lam, J. W. Y.; Dong, Y.; Yuan, W.; Sun, J.; Hua, J.; Wong, K. S.; Tang, B. Z. *Macromolecules* **2006**, *39*, 467. (d) Masuda, T. *J. Polym. Sci., Part A: Polym. Chem.* **2007**, *45*, 165. (e) Tang, B. Z. *Macromol. Chem. Phys.* **2008**, *209*, 1303. (f) Li, C.; Li, Y. *Macromol. Chem. Phys.* **2008**, *209*, 1541. (g) Sanchez, J. C.; Trogler, W. C. *Macromol. Chem. Phys.* **2008**, *209*, 1527. (h) Rudick, J.; Percec, V. *Macromol. Chem. Phys.* **2008**, *209*, 1759. (i) Kwak, G.; Jin, S.-H.; Park, J.-W.; Gal, Y.-S. *Macromol. Chem. Phys.* **2008**, *209*, 1769. (j) Su, X. Y.; Xu, H. Y.; Guo, Q. Z.; Shi, G.; Yang, J. Y.; Song, Y. L.; Liu, X. Y. *J. Polym. Sci., Part A: Polym. Chem.* **2008**, *46*, 4529.

(7) For example, see (a) Stolka, M.; Yanus, J.; Pai, D. *J. Phys. Chem.* **1984**, *88*, 4707. (b) Strohriegl, P.; Grazulevicius, J. V. *Adv. Mater.* **2002**, *14*, 1439. (c) Ego, C.; Grimsdale, A. C.; Weil, T.; Enkelmann, V.; Müllen, K. *Adv. Mater.* **2002**, *14*, 809. (d) He, Q. G.; Lin, H. Z.; Weng, Y. F.; Zhang, B.; Wang, Z. M.; Lei, G. T.; Wang, L. D.; Qiu, Y.; Bai, F. L. *Adv. Funct. Mater.* **2006**, *16*, 1343. (e) Deng, L.; Furuta, P. T.; Garon, S.; Li, J.; Kavulak, D.; Thompson, M. E.; Fréchet, J. M. J. *Chem. Mater.* **2006**, *18*, 386.

(8) (a) Qu, J. Q.; Kawasaki, R.; Shiotsuki, M.; Sanda, F.; Masuda, T. *Polymer* **2006**, *47*, 6551. (b) Katsumata, T.; Maitani, M.; Huang, C. C.; Shiotsuki, M.; Masuda, T. *Polymer* **2008**, *49*, 2808.

(9) Qu, J. Q.; Suzuki, Y.; Shiotsuki, M.; Sanda, F.; Masuda, T. *Polymer* **2007**, *48*, 4628.

(10) Sun, R.; Masuda, T.; Kobayashi, T. *Synth. Met.* **1997**, *91*, 301.

(11) Wang, P. F.; Wu, S. K. *J. Photochem. Photobiol., A* **1993**, *76*, 27.

(12) Marcus, R. A. *Annu. Rev. Phys. Chem.* **1964**, *15*, 155.

(13) (a) Lippert, E. *Z. Naturforsch., A: Phys. Sci.* **1955**, *10*, 541. (b) Mataga, N.; Kaifu, Y.; Koizumi, M. *Bull. Chem. Soc. Jpn.* **1956**, *29*, 465. (c) Qin, A. J.; Lam, J. W. Y.; Dong, H. C.; Lu, W. X.; Jim, C. K. W.; Dong, Y. Q.; Haussler, M.; Sung, H. H. Y.; Williams, I. D.; Wong, G. K. L.; Tang, B. Z *Macromolecules* **2007**, *40*, 4879.

(14) (a) Grigalevicius, S. *Synth. Met.* **2006**, *156*, 1. (b) Shirota, Y. *J. Mater. Chem.* **2005**, *15*, 75. (c) Xu, W. J.; Chen, H. Z.; Shi, M. M.; Huang, G. Y.; Wang, M. *Nanotechnology* **2006**, *17*, 728.

(15) Tang, B. Z.; Chen, H.; Xu, R.; Lam, J. W. Y.; Cheuk, K. K. L.; Wong, H. N. C.; Wang, M. *Chem. Mater.* **2000**, *12*, 213.

(16) Borsenberger, P. M.; Weiss, D. S. *Organic Photoreceptors for Imaging Systems*; Marcel Dekker: New York, 1993.

(17) Varanasi, P. R.; Jen, A. K.; Chandrasekhar, Y. J.; Namboothiri, I. N. N.; Rathna, A. *J. Am. Chem. Soc.* **1996**, *118*, 12443.

(18) (a) Sun, J. Z.; Chen, H. Z.; Xu, R. S.; Wang, M.; Lam, J. W. Y.; Tang, B. Z. *Chem. Commun.* **2002**, 1222. (b) Xu, H.-P.; Shi, M.-M.; Chen, H.-Z.; Wang, M.; Tang, B. Z. *Chin. J. Polym. Sci.* **2005**, *23*, 675. (c) Xu, H. P.; Sun, J. Z.; Qin, A. J.; Hua, J. L.; Li, Z.; Dong, Y. Q.; Xu, H.; Yuan, W. Z.; Ma, Y. G.; Wang, M.; Tang, B. Z. *J. Phys. Chem. B* **2006**, *110*, 21701.

(19) (a) Schrock, R. R.; Osborn, J. A. *Inorg. Chem.* **1970**, *9*, 2339. (b) Tang, B. Z.; Poon, W. H.; Leung, S. M.; Leung, W. H.; Peng, H. *Macromolecules* **1997**, *30*, 2209.

(20) Huang, H. M.; He, Q. G.; Lin, H. Z.; Bai, F. L.; Sun, Z.; Li, Q. S. *Polym. Adv. Technol.* **2004**, *15*, 84.

MA8014323